Title

CaMn3IVO4 Cubane Models of the Oxygen-Evolving Complex: Spin Ground States S<9/2 and the Effect of Oxo Protonation

Journal

Angewandte Chemie International Edition, 60(32)

ISSN

1433-7851

Authors

Lee, Heui Beom
Shiau, Angela A
Marchiori, David A
et al.

Publication Date

2021-08-02

DOI

10.1002/anie.202105303

Peer reviewed

Published in final edited form as:

Angew Chem Int Ed Engl. 2021 August 02; 60(32): 17671–17679. doi:10.1002/anie.202105303.

$CaMn_3^{IV}O_4$ Cubane Models of the Oxygen Evolving Complex: Spin Ground States $S < 9/2$ and the Effect of Oxo Protonation

Heui Beom Lee[a], **Angela A. Shiau**[a], **David A. Marchiori**[b], **Paul H. Oyala**[a], **Byung-Kuk Yoo**[a], **Jens T. Kaiser**[a], **Douglas C. Rees**[a], **R. David Britt**[b], **Theodor Agapie**[a]

[a]Department of Chemistry and Chemical Engineering, California Institute of Technology, 1200 E California Blvd MC 127-72, Pasadena, CA 91125, United States

[b]Department of Chemistry, University of California, Davis, One Shields Ave, Davis, California 95616, United States

Abstract

We report single crystal XRD and MicroED structure, magnetic susceptibility, and EPR data of a series of $CaMn_3^{IV}O_4$ and $YMn_3^{IV}O_4$ complexes as structural and spectroscopic models of the cuboidal subunit of the OEC. The effect of changes in heterometal identity, cluster geometry, and bridging oxo protonation on spin state structure was investigated. In contrast to previous computational models, we show that the spin ground state of $CaMn_3^{IV}O_4$ complexes and variants with protonated oxo moieties need not be $S = 9/2$. Desymmetrization of the *pseudo*-C_3 symmetric $Ca(Y)Mn_3^{IV}O_4$ core leads to a lower $S = 5/2$ spin ground state. The magnitude of the magnetic exchange coupling is attenuated upon oxo protonation, and an $S = 3/2$ spin ground state is observed in $CaMn_3^{IV}O_3(OH)$. Our studies complement the observation that the interconversion between the low spin and high spin forms of the S_2 state is *p*H dependent, suggesting that (de)protonation of bridging or terminal oxygen atoms in the OEC may be connected to spin state changes.

Graphical Abstract

agapie@caltech.edu.

Supporting information for this article is given via a link at the end of the document.

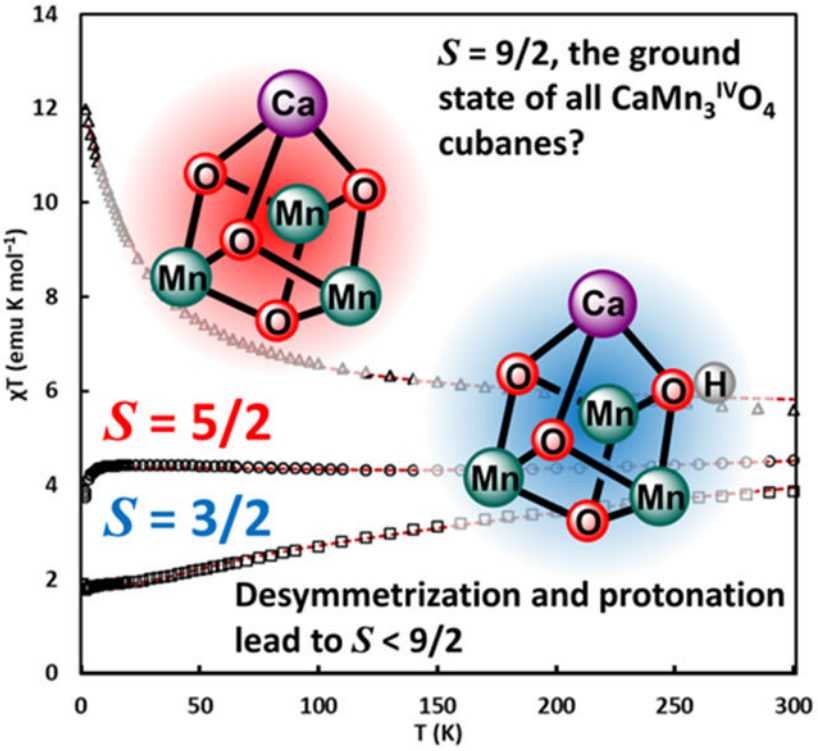

To better describe the electronic structure of the S_n state intermediates of Photosystem II, a ferromagnetically coupled $CaMn_3^{IV}O_4$ subunit with an $S = 9/2$ ground state has been proposed. This assignment has played a key role in the mechanism of water oxidation, but structure–electronic structure studies of $CaMn_3^{IV}O_4$ complexes remain rare. Through cluster desymmetrization or oxo protonation, lower spin ground states are found to be accessible, challenging prior models.

Keywords

oxygen evolving complex; model complex; electronic structure; magnetic susceptibility; spin state

Introduction

Biological water oxidation is catalyzed at the oxygen evolving complex (OEC) of Photosystem II.[1-3] The OEC has been characterized by crystallography, revealing a heterometallic $CaMn_3O_4$ cubane motif binding to a fourth Mn center via bridging (hydr)oxo moieties.[4-6] Mechanistic studies have been performed within the context of the Joliot-Kok cycle of S_n ($n = 0$~4) states.[7-8] Starting from the dark-stable S_1 state ($Mn_2^{III}Mn_2^{IV}$), light-induced one e^- oxidation leads to the formation of the S_2 state, and numerous studies have been performed to better understand the (electronic) structure of the S_2 state and the requirements needed to advance to the higher S_n states.[9-19] In the absence of unambiguous and direct structural data concerning the O—O bond forming S_4 intermediate, structural and spectroscopic characterization of lower S_n state intermediates influence mechanistic proposals for O—O bond formation.[20-24]

Connected to Mn oxidation state and structural changes, each of the S_n state intermediates adopts a unique electronic structure with a characteristic spin ground state S_G:[25] $S_G(S_0)$ = 1/2,[26] $S_G(S_1)$ = 0[27] or higher[28-29], $S_G(S_2)$ = 1/2 or 5/2,[30-32] $S_G(S_3)$ = 3.[15, 33-35] The interconversion between the S_G = 1/2 and S_G = 5/2 forms of the S_2 state is notable.[30] One interpretation invokes structural changes in the $CaMn_4$ core centered around the location of a particular O(5) oxo moiety, with concomitant changes in the magnetic coupling interactions resulting in a different S_G.[13] In the so-called "closed-cubane" structure with S_G = 5/2, ferromagnetic coupling between Mn(1), Mn(2), and Mn(3) is proposed to lead to an S = 9/2 spin state for the $CaMn_3^{IV}O_4$ cuboidal subunit; antiferromagnetic coupling to the dangling Mn(4) would lead to the observed S_G = 5/2 (Figure 1). In the "open-cubane" structure where O(5) bridges Mn(3) and Mn(4) instead, an internal valence redistribution is proposed, with the $CaMn^{III}Mn_2^{IV}$ subsite now proposed to have an S = 1 spin state; antiferromagnetic coupling to the dangling Mn(4) would lead to the observed S_G = 1/2.[13, 25] The above structural isomerism model helps explain the high- and low-spin forms of the S_2 state. Importantly, however, the model depends on the closed-cubane motif (region within the red box, Figure 1) having a ferromagnetically coupled S = 9/2 spin state. At room temperature, under turnover conditions, only the open-cubane form has been observed crystallographically thus far.[6, 36] While experimental data remains very limited, two synthetic $CaMn_3^{IV}O_4$ model complexes have been reported with S_G = 9/2 (Figure 2),[37-39] supporting the coupling scheme for the closed-cubane structure and the possible structural flexibility of the OEC core as an explanation for the spin state interconversion observed in the S_2 state. Subsequent XFEL structural studies show the incorporation of a sixth oxygen O(6) in the cleft between Mn(1) and Mn(4), a possible site for O—O bond formation (Figure 1).[6] A similar magnetic coupling scheme has been advanced for the S_3 state (Mn_4^{IV}), featuring a ferromagnetically coupled $CaMn_3^{IV}O_4$ subunit with an S = 9/2 spin state; antiferromagnetic coupling to Mn(4) would lead to the observed S_G = 3 (Figure 1).[15, 40] Similar to the S_2 state, a structural interpretation for the observed spectral heterogeneity in the S_3 state is the subject of ongoing investigation.[34] An alternative interpretation for the spin state interconversion in the S_2 state is based on the observation that this process is *p*H dependent, with a higher *p*H favoring the high-spin ground state.[24, 41] Notably, other effects such as low temperature irradiation of the S_1 state and the introduction of F^- favor formation of the high-spin state.[42-43] Insofar as the *p*H effect, the aquo moiety bound to Mn(4) was hypothesized to be the site that is deprotonated following the observation that no *p*H dependent behavior is observed when NH_3 is bound to this aquo site.[17, 24, 41] Structural changes to the OEC through either oxo exchange or (de)protonation would be accompanied by concomitant changes in the nature and magnitude of the magnetic exchange coupling *J*, which in turn affect not only the S_G of the cluster but also other spectroscopic properties such as the sign and magnitude of the projected ^{55}Mn hyperfine coupling constants.[15, 39, 44] In a related computational study, protonation of the bridging oxo O(4) (Figure 1) in the S_2 state is proposed to lead to a high spin state, while maintaining the open-cubane structure.[24] XAS studies performed on the high-spin form of the S_2 state indeed show structural differences to the low-spin form, but extracted Mn-Mn distances do not appear consistent with the closed-cubane structure.[18] Such computational and experimental discrepancies highlight the need for data on model compounds in which mechanistic hypotheses can be

tested and the effects of structural changes on the electronic structure of the OEC can be evaluated.

Despite significant synthetic efforts to prepare heterometallic complexes that mimic the OEC in terms of structure and redox state,[37, 45-58] the effect of structural distortions or protonation state on the electronic structure of multimetallic Mn complexes is not well understood, and can be summarized as follows.[59-63] In a series of dinuclear complexes featuring $Mn_2^{IV}O_2$, $Mn_2^{IV}O(OH)$, and $Mn_2^{IV}(OH)_2$ cores, the antiferromagnetic coupling is strongest in the fully deprotonated form, with successive oxo protonations resulting in weaker antiferromagnetic coupling.[60] A complete shift from ferromagnetic to antiferromagnetic coupling is observed upon a single protonation of the adamantane-shaped $[Mn_4^{IV}O_6]^{4+}$ core.[59] While representing incomplete models of the OEC, $CaMn_3^{IV}O_4$ complexes offer an opportunity to better understand the magnetic properties of the OEC, as it relates to current discussions on the geometry and the spin state of the S_2 state. Any changes to the spin state of the cubane portion would result in a different total spin of the cofactor when magnetically coupled to the dangler Mn(4). The ground state of both the *pseudo-*C_3 symmetric and the Ca-bound asymmetric $Ca_2Mn_3^{IV}O_4$ model complexes has been assigned to $S_G = 9/2$ on the basis of magnetic, spectroscopic, and computational data (Figure 2).[37-38, 49, 64] Subsequent computational studies concluded that the spin ground state of cuboidal $CaMn_3^{IV}O_4$ complexes and all possible protonated analogues $CaMn_3^{IV}O_n(OH)_{(4-n)}$ (n = 0~4) is $S_G = 9/2$.[64] Studies that probe the effect of distinct structural changes or oxo protonation on the electronic structure of $CaMn_3^{IV}O_4$ complexes have not been reported.

Herein, we report single crystal XRD and MicroED structure, magnetic susceptibility, and EPR data of a series of cuboidal complexes featuring $CaMn_3^{IV}O_4$, $YMn_3^{IV}O_4$, and $CaMn_3^{IV}O_3(OH)$ cores. Our results show that the electronic structure of $CaMn_3^{IV}O_4$ complexes is highly sensitive to changes promoted by the nature of the supporting ligands (reminiscent to studies of $Mn^{III}Mn_3^{IV}O_4$ complexes)[65] and the protonation state. We show that ground states such as $S_G = 5/2$ and $S_G = 3/2$ are possible in $CaMn_3^{IV}O_4$ complexes, which challenge the proposed model that a closed cubane such as that in the S_2 state of the OEC must be $S_G = 9/2$.

Results and Discussion

Synthesis and crystal structure.

The acetate-bridged complex **1-Ca** was used as a precursor for other complexes (Scheme 1).[37] Magnetic susceptibility and computational studies on **1-Ca** indicate an $S_G = 9/2$ ground state.[38, 64] Treatment of **1-Ca** with $Y(OTf)_3$ leads to the analogous complex **1-Y**.[50] Magnetic studies show that **1-Y** has a similar $S_G = 9/2$.[66] Desymmetrization of the *pseudo-*C_3 symmetric complexes **1-Ca** and **1-Y** was achieved via substitution of two acetate moieties with a chelating bis-oxime proligand ($H_2N_4O_2$). Treatment of **1-Ca** with $H_2N_4O_2$ results in the formation of **2-Ca** via a protonolysis reaction.[67] Similarly, treatment of **1-Y** with $H_2N_4O_2$ results in the formation of the analogous complex **2-Y**.[58] Due to its limited solubility, suitable samples of **2-Ca** for single crystal X-ray diffraction studies could not be obtained. The structure of **2-Ca** was determined using MicroED.[68] A powder sample of **2-**

Ca was judiciously treated with MeCN to obtain a TEM grid with non-aggregated particles of **2-Ca** without loss of crystallinity. Complex **2-Ca** dissolves in MeCN only sparingly, which is critical in obtaining a TEM grid with dispersed but intact microcrystals. The resolution and refinement parameters of **2-Ca** were similar to those obtained for other MicroED organometallic structures (Table S4).[68] Importantly, the MicroED structure of **2-Ca** shows that the $CaMn_3O_4$ core is preserved, with a coordination sphere that is analogous to that of **2-Y**.[58, 67] The $CaMn_3O_4$ core of **2-Ca** can be further desymmetrized via treatment with 2,6-lutidinium triflate, which results in the protonation of a unique oxo in between the oximate moieties to afford a complex with a $CaMn_3O_3(OH)$ core (**3-Ca**).

Toward expanding the series of $CaMn_3O_4$ complexes with chelating ligands of similar basicity to the oximate moieties, an amidate-bridged complex was targeted. Treatment of **1-Ca** with a triethylene glycol derived bis-amide (H_2diam) in the presence of NaO^{t}Bu leads to the formation of **4-Ca**. The crystal structure of **4-Ca** is consistent with the $LCaMn_3O_4$(diam)(OAc) formulation in which two acetate moieties of **1-Ca** are replaced by the chelating bis-amidate moiety (Figure 3). Overall, **1-Ca(Y)**, **2-Ca(Y)**, **3-Ca**, and **4-Ca** represent a unique series of complexes mimicking the cuboidal substructure of the OEC in which cluster symmetry, heterometal identity, bridging ligand, and oxo protonation state is systematically varied.

Metal-oxo distances were compared across the series to understand the effect of chelating ligands and oxo protonation on structure (Table S1). Within each complex **1-Ca** or **4-Ca**, Ca-oxo, Mn-Mn, and M-O(4) distances are all similar to each other; the other six Mn-oxo distances alternate between 1.83 and 1.87 Å along the *pseudo-C_3* axis of symmetry parallel to the Ca-O(4) vector. A similar *pseudo-C_3* symmetry is observed in **1-Y** and in other known analogues such as **1-Gd**.[50] The high symmetry of the metal-oxo core is broken with the oximate-bridged complexes. Because precise structural metrics could not be obtained from the MicroED structure of **2-Ca**, the structure of **2-Y** was used as a surrogate for the structure of **2-Ca** for structural comparisons. Notably, the structure of **2-Y** and the Gd analogue **2-Gd** are very similar to each other, with Mn-oxo distances within 0.01 Å, indicating that general structural trends are observable. In **2-Y**, the Y-O(1) distance is significantly shorter by 0.1 Å than the other two Y-oxo distances. O(1) is the unique oxo that is located between the two oximate donors, suggesting that the metal-oxo core has been structurally and electronically desymmetrized. While the difference is smaller, the Mn-oxo distances trans to the Mn-oximate bonds are slightly elongated compared to the corresponding Mn-oxo distance trans to the Mn-acetate/amidate bond. Similarly, Mn-Mn distances in **2-Y** also distort in a manner that is consistent with a *pseudo-C_S* symmetry with the mirror plane containing the Y(1)–O(1) vector and bisecting the Mn(1)–Mn(2) vector. On the basis that the three-fold symmetry of **1-Y**(**Gd**) is broken upon substitution of two acetates with the bridging oxime $H_2N_4O_2$, a similar structural distortion is expected in **2-Ca**, away from the *pseudo-C_3* symmetry of **1-Ca**. The structure of **3-Ca** is also consistent with a *pseudo-C_S* symmetry, with Mn-(μ^3-OH) distances that are slightly elongated by roughly 0.1 Å in comparison to the corresponding Mn-(μ^3-O) distances in **1-Ca**. Overall, distinct structural changes are observed depending on the nature of the bridging ligands and the protonation state of

bridging oxos; these relatively small structural changes across the series have a significant influence in the electronic structure of the $CaMn_3^{IV}O_4$ core.

Magnetometry.

To obtain insight into the electronic structure of the series of $CaMn_3^{IV}$ complexes, magnetic susceptibility studies were performed (Figure 4). For a *pseudo-*C_S symmetric Mn_3^{IV} core, an isotropic spin exchange Hamiltonian (eq 1) with two distinct magnetic interactions can be employed, with a unique $J' = J_{12}$ and $J = J_{13} = J_{23}$ (subscripts follow the Mn numbering scheme in Figure 3).[69] For Mn_3^{IV} systems with local spin $S_i = 3/2$, application of the vector coupling model $S' = S_1 + S_2$, $S_T = S' + S_3$ gives rise to twelve $|S_T, S'\rangle$ states, in which S' varies in integer increments from 0 to $2S_i$ (i.e. $S' = 0, 1, 2, 3$); for each value of S', S_T varies in integer increments from $|S' - S_i|$ to $S' + S_i$ (i.e. for $S' = 3$, $S_T = 3/2, 5/2, 7/2, 9/2$). The energies of the individual $|S_T, S'\rangle$ states can be expressed as shown in eq 2. By incorporating the energies of the twelve $|S_T, S'\rangle$ states into the Van Vleck equation, an analytical solution for the magnetic susceptibility X can be obtained. Qualitatively, one can regard X to be derived from the sum of the individual $|S_T, S'\rangle$ states weighed by their Boltzmann populations. At sufficiently low temperatures where only the ground state is significantly populated, reduced magnetization studies can be performed to obtain information about zero field splitting. Finally, while the relative energies of the individual states depend on the sign and magnitude of J and J', the ground state is more easily determined from the ratio of J/J' (Figure 5).[49, 64]

$$\widehat{H} = -2J(S_1S_3 + S_2S_3) - 2J'S_1S_2 \quad (1)$$

$$E \mid S_\tau, S'\rangle = -JS_\tau(S_\tau + 1) - (J' - J)S'(S' + 1) \quad (2)$$

Structurally most similar to **1-Ca**, **4-Ca** was studied by magnetometry (Figure 4a). The XT value (units of emu K mol^{-1}) of 5.60 at 300 K increases with cooling to reach a maximum XT value of 11.98 at 2 K. This maximum value is in good agreement with the expected value of 12.375 for $S_G = 9/2$ ($g = 2$). Previous magnetic studies on **1-Ca** show that while the structure is more consistent with a *pseudo-*C_3 symmetry, the data is better fit with two values $J = 3.5$ cm^{-1} and $J' = -1.8$ cm^{-1}.[38] The data for **4-Ca** was similarly fit with two values $J = 5.0$ cm^{-1}, $J' = -1.6$ cm^{-1}, and $g = 1.97$. Using the fitted J values, the relative energies of the individual electronic states can be calculated. The $|9/2, 3\rangle$ ground state is separated from the $|7/2, 2\rangle$ first excited state by 5.5 cm^{-1} and from the $|5/2, 1\rangle$ second excited state by 8.8 cm^{-1}. The small separation between the ground and excites states is evident in the fact that XT decreases sharply from the maximum value upon warming. The J/J' ratio of −3.125 is fully consistent with $S_G = 9/2$ and comparable to the value of −3.75 obtained for the asymmetric $Ca_2Mn_3^{IV}O_4$ complex.[49] The reduced magnetization data for **4-Ca** (Figure 4d) shows little deviation from the ideal Brillouin function for $S = 9/2$, indicating the presence of a small zero-field splitting estimated at $D = -0.1$ cm^{-1} by EPR. Magnetic studies on **4-Ca** show that changing the bridging ligands from acetates to amidates does not result in significant changes to the electronic structure of the complex in the absence of notable structural distortions to the metal-oxo core.

Featuring a lower symmetry, distorted metal-oxo core compared to **1-Ca** and **4-Ca**, **2-Ca** was studied by magnetometry (Figure 4a). The XT value of 4.526 at 300 K decreases slowly to a local minimum XT value of 4.313 at 150 K. Upon further cooling, the XT value increases slowly to reach a value of 4.405 at 15 K, in good agreement with the expected value of 4.375 for $S_G = 5/2$ ($g = 2$). Further decrease in XT with temperature can be attributed to intermolecular antiferromagnetic interactions and/or zero-field splitting. The temperature dependence of XT observed in **2-Ca** is indicative of an irregular spin state structure where the first excited state is $S \leq 3/2$ and the second excited state is $S \geq 5/2$. Similar magnetic behavior has been observed in other trinuclear systems.[70-73] On the basis of the small curvature of the XT vs. T curve, the expected separation between the spin ground state and the first excited state is in the order of hundreds of wavenumbers. To simulate the susceptibility data, the following parameters were used: $g = 1.99$, $J = 250 \pm 50$ cm^{-1}, $J' = -280 \pm 50$ cm^{-1}. Due to the small curvature of the XT vs. T curve, a relatively large variance is reported for the J values, which should not be treated as exact values but as estimates. However, the range in the J/J' ratio is narrower, between −0.90 and −0.93, and falls within the predicted region for $S_G = 5/2$ (Figure 5).[64] The $|5/2, 1\rangle$ ground state is separated from the $|3/2, 0\rangle$ first excited state by 210 ± 50 cm^{-1} and from the $|7/2, 2\rangle$ second excited state by 350 ± 50 cm^{-1}. Thermally well-isolated spin ground states have been observed in multinuclear complexes, with values of $|J|$ in the range of 160~900 cm^{-1}.[74-76] Such systems behave as Curie paramagnets, with no temperature dependence of XT. In the absence of double exchange or close metal-metal contacts, the physical nature of the large increase of J in **2-Ca** remains unclear, but we provide the following hypothesis. In **1-Ca** and **4-Ca** where each Mn(IV) ion is coordinated by mostly σ-only ligands, the principal symmetry axis for each Mn center is ill-defined, and thus several competing exchange pathways can be envisioned between d_{xy}, d_{xz}, and d_{yz}, resulting in the overall weak coupling observed. In **2-Ca** and **2-Y**, in contrast, Mn(1) and Mn(2) are coordinated by oximates which may act as pπ-donors (also more basic σ-donors than carboxylates). This defines the Mn-O(oxime) vector as the z axis for Mn(1) and Mn(2). Because d_{xz} and d_{yz} may be involved in dπ-pπ bonding with the oximates, contributions from exchange pathways such as $(d_{xy})^1|O|(d_{xz})^1$ that weaken the overall magnitude of the antiferromagnetic coupling may be reduced. The exchange pathway through the geometrically "aligned" d_{xy} orbitals on Mn(1) and Mn(2) may explain the larger J. For **2-Ca**, the reduced magnetization isofield at 7 T reaches a value of 4.71 $N_A\mu_B$ at 1.8 K, consistent with $S_G = 5/2$ (Figure 4b). Reduced magnetization isofields were simulated assuming a single value of $D = +1.46$ cm^{-1} or -1.17 cm^{-1}. In many cases, powder susceptibility data is insensitive to the sign of D.[77] This value of D is inconsistent with the value obtained from EPR, at 0.3 cm^{-1} (Figure 6a). Using this value instead and incorporating the mean field model of intermolecular antiferromagnetic interaction zJ, a satisfactory fit can be obtained (Figure S7). The magnetic data on **2-Y**, for which a high resolution crystal structure has been obtained, is also consistent with $S_G = 5/2$, showing that the change in the spin ground state from $S_G = 9/2$ to $S_G = 5/2$ is also observed going from **1-Y** to **2-Y** (Figure S8). The data on **2-Y** was simulated with the following parameters: $g = 2.0$, $J = 280 \pm 50$ cm^{-1}, $J' = -315 \pm 55$ cm^{-1}, $J/J' = -0.89$. Importantly, magnetic studies on **2-Ca** show that an intact $CaMn_3^{IV}O_4$ cubane moiety need not necessarily have an $S_G = 9/2$ ground state.

Featuring a bridging hydroxo moiety, **3-Ca** was studied by magnetometry (Figure 4). The XT value of 3.856 at 300 K decreases monotonically with temperature to reach a value of 1.886 at 10 K, in good agreement with the expected value of 1.875 for $S_G = 3/2$ ($g = 2$). To simulate the susceptibility data, the following parameters were used: $g = 2.0$, $J = +11$ cm^{-1}, $J' = -55$ cm^{-1}. The J/J' ratio of −0.2 falls within the predicted region for $S_G = 3/2$ (Figure 5).[64] The $|3/2, 0\rangle$ ground state is separated from the $|5/2, 1\rangle$ first excited state by 77 cm^{-1} and from the $|3/2, 1\rangle$ second excited state by 132 cm^{-1}. Similar to **4-Ca**, magnetization studies show little deviation from the ideal Brillouin function for $S = 3/2$, indicating the presence of a small zero-field splitting (Figure 4c). Importantly, magnetic studies on **3-Ca** show that protonation of a single bridging oxo moiety has a strong influence in attenuating the magnitude of the magnetic coupling interactions.[60] While protonation of **2-Ca** does not change the nature (sign) of the magnetic coupling interactions in **3-Ca**, the relative magnitudes of J and J' result in a change of spin ground state, from $S_G = 5/2$ in **2-Ca** to $S_G = 3/2$ in **3-Ca**. In a tetranuclear Mn_4 system, a complete reversal from ferromagnetic to antiferromagnetic interactions has been reported.[59] With a structure that closely resembles the closed-cubane subunit of the OEC, the spin state of **3-Ca** differs from the predicted $S_G = 9/2$, and an $S_G = 3/2$ is observed.[64] To obtain magnetostructural insight for the observed changes in spin ground state, the geometry of the Mn(1)-O(1/4)-Mn(2) subsite was closely examined. Mn(1)-O-Mn(2) angles increase slightly going from the *pseudo*-C_3 symmetric complex **1-Ca** to the desymmetrized complex **2-Y** (Table S2). A comparably more dramatic increase in the Mn-O-Mn angles is observed in the protonated complex **3-Ca**. The observed trend of increasing Mn-O-Mn angles is consistent with the decrease in spin ground state within the series, and can be explained in the context of an increased antiferromagnetic exchange for a more linear Mn-O-Mn linkage. Complex **3-Ca** with the widest Mn-O-Mn angles therefore has the smallest J/J' ratio and the lowest spin state. Most importantly, magnetic studies show that spin states such as $S_G = 5/2$ and 3/2 are possible for a closed-cubane structure.

EPR spectroscopy.

To obtain further insight into the electronic structure of complexes **2-Ca**, **3-Ca**, and **4-Ca**, X-band EPR studies were conducted (Figure 6). Qualitatively, the spectrum of **2-Ca** suggests that the weak field regime is operative, ($D \gg h\nu \approx 0.3$ cm^{-1} at X-band), where D is the axial component of the zero-field splitting (ZFS) parameter. In such cases, as illustrated in the rhombograms for half-integer spin states $S > 1/2$, peak positions are primarily determined by the E/D ratio where E is the transverse component of the ZFS parameter. The spectrum of **2-Ca** features three transitions at $g = 6.3$ (108 mT), $g = 4.3$ (160 mT), and $g = 2$ (340 mT) that can be assigned to the $|\pm 1/2\rangle$ Kramers doublet of an axial ($E/D \approx 0$) $S = 5/2$. The spectrum of **2-Ca** can be approximated using parameters that are consistent with this qualitative analysis (Figure 6a). The broad spectrum of **2-Ca** was simulated with a Gaussian distribution of E/D centered at 0.06 with a full width at half-maximum of 0.03 (Figure S9). The spectrum of **2-Y** is similar to that of **2-Ca**, consistent with the magnetic data showing that both have an $S_G = 5/2$ ground state (Figure S10). The spectrum of **3-Ca** features two main transitions at $g = 5.1$ (133 mT) and $g = 2.1$ (330 mT) that can be assigned to the $|\pm 1/2\rangle$ Kramers doublet of a rhombic ($E/D \approx 0.3$) $S = 3/2$ (Figure 6b). While not amenable for a simple qualitative analysis, the spectrum of **4-Ca** suggests a higher $S_G = 9/2$ with multiple

overlapping transitions from the five Kramers doublets and is reminiscent of the spectrum of the $Ca_2Mn_3O_4$ complex with an $S_G = 9/2$ ground state (Figure 6c).[49] The ZFS parameters of **4-Ca** were obtained by simultaneously fitting spectra obtained at X- and D-band (130 GHz). At higher microwave frequencies, the electron Zeeman term that splits the energy levels of a spin system in an applied magnetic field may be appreciably larger than that of the ZFS parameter. This is the case for **4-Ca** at 130 GHz, where hv >> *D*. In such cases, the resulting EPR spectrum is centered around the *g* value that defines the total spin system. The width of the spectrum is determined by *D*, while the spacing of the EPR transitions is determined by *E/D*. The D-band electron-spin echo EPR spectrum of **4-Ca** (Figure S11) displays approximately nine transitions centered about $g = 1.99$ and spans approximately 1.5 T. The transitions that appear at magnetic fields lower than 4.67 T ($g = 1.99$) are evenly spaced by approximately 200 mT, while those at fields higher than 4.67 T are unevenly spaced. This is consistent with a small, negative ZFS parameter ($D = -0.1\ cm^{-1}$) that is axial ($E/D = 0.11$). Overall, EPR spectroscopic studies of **2-Ca**~**4-Ca** are consistent with the electronic structure and spin ground state description obtained from magnetic susceptibility studies.

Conclusion

In summary, a series of $CaMn_3^{IV}O_4$ cuboidal complexes has been synthesized and characterized by XRD/MicroED, magnetometry and EPR spectroscopy. To our knowledge this is the first set of experimental studies that directly addresses the effect of systematic changes in cluster geometry and bridging oxo protonation on the spin state structure of $CaMn_3^{IV}O_4$ cubane models of the OEC. With implications in the interpretation of OEC spectroscopic properties, our benchmarking results show that the electronic structure of the $CaMn_3^{IV}$ core is highly sensitive to small geometric changes, nature of the bridging ligands, and protonation state of the bridging oxo moieties. Even in the absence of large oxo movements proposed to account for the high spin and low spin signals of the S_2 state of the OEC, we find that spin ground states such as $S_G = 3/2$, 5/2, or 9/2 are accessible for the $CaMn_3^{IV}$ subsite (Figure 4). Importantly, desymmetrization of *pseudo*-C_3 symmetric complexes **1-Ca**(**1-Y**) and **4-Ca** with $S_G = 9/2$ lead to a lower, $S_G = 5/2$ in **2-Ca**(**2-Y**). Protonation of a single bridging oxo moiety in **2-Ca** has a strong influence in attenuating the magnitude of the magnetic exchange coupling interactions, and $S_G = 3/2$ is observed in **3-Ca**. The nature of the magnetic exchange interactions does not need to change to result in a different spin ground state; differences in the relative ratio of *J* values can lead to different ground states (Figure 5). Our results strongly argue against the idea that the ground state of $CaMn_3^{IV}O_n(OH)_{(4-n)}$ ($n = 0$~4) complexes must necessarily be $S_G = 9/2$ as previously reported; the protonation of a single bridging oxo may result in spin ground state changes in tetranuclear complexes.[64] Nevertheless, while the present results demonstrate that closed $CaMn_3^{IV}O_n(OH)_{(4-n)}$ cubane motifs can have spin states different from $S_G = 9/2$, they do not rule out such an interpretation for the $CaMn_3^{IV}$ subunit of the OEC. However, they do add support to mechanistic proposals that do not require structural distortions of the overall cluster for the observation of additional spin states. For example, recent *p*H dependence studies show that the $S_G = 1/2$ form of the S_2 state converts to the $S_G = 5/2$ form at high *p*H.[41-42] On the basis of the results presented in this study, we support an interpretation based

on spin state changes following deprotonation of a bridging hydroxo or terminal aquo. Most importantly, our results indicate that interpretation of EPR signals and subsequent structural assignments should not be limited to an $S = 9/2$ spin state for the $CaMn_3^{IV}O_4$ subsite of the OEC.

Supplementary Material

Refer to Web version on PubMed Central for supplementary material.

Acknowledgements

This research was supported by the NIH (R01-GM102687B to T.A.), Dow Next Generation Educator (instrumentation), NSF-1531940 (Caltech EPR facility), the Division of Chemical Sciences, Geosciences, and Biosciences (R.D.B. grant DE-SC0007203) of the Office of Basic Energy Sciences of the U.S. Department of Energy. We thank Dr. Michael K. Takase and Mr. Lawrence M. Henling at Caltech for assistance with XRD; Dr. Ignacio B. Martini at UCLA for assistance with magnetometry (NSF, MRI-1625776).

References

[1]. Yano J, Yachandra V, Chem. Rev 2014, 114, 4175–4205. [PubMed: 24684576]

[2]. Shen J-R, Annu. Rev. Plant Biol 2015, 66, 23–48. [PubMed: 25746448]

[3]. Pantazis DA, ACS Catal. 2018, 8, 9477–9507.

[4]. Umena Y, Kawakami K, Shen J-R, Kamiya N, Nature 2011, 473, 55. [PubMed: 21499260]

[5]. Suga M, Akita F, Hirata K, Ueno G, Murakami H, Nakajima Y, Shimizu T, Yamashita K, Yamamoto M, Ago H, Shen J-R, Nature 2014, 517, 99. [PubMed: 25470056]

[6]. Kern J, Chatterjee R, Young ID, Fuller FD, Lassalle L, Ibrahim M, Gul S, Fransson T, Brewster AS, Alonso-Mori R, Hussein R, Zhang M, Douthit L, de Lichtenberg C, Cheah MH, Shevela D, Wersig J, Seuffert I, Sokaras D, Pastor E, Weninger C, Kroll T, Sierra RG, Aller P, Butryn A, Orville AM, Liang M, Batyuk A, Koglin JE, Carbajo S, Boutet S, Moriarty NW, Holton JM, Dobbek H, Adams PD, Bergmann U, Sauter NK, Zouni A, Messinger J, Yano J, Yachandra VK, Nature 2018.

[7]. Joliot P, Biochimica et Biophysica Acta (BBA) - Biophysics including Photosynthesis 1965, 102, 116–134.

[8]. Kok B, Forbush B, McGloin M, Photochemistry and Photobiology 1970, 11, 457–475. [PubMed: 5456273]

[9]. Ames W, Pantazis DA, Krewald V, Cox N, Messinger J, Lubitz W, Neese F, J. Am. Chem. Soc 2011, 133, 19743–19757. [PubMed: 22092013]

[10]. Su J-H, Cox N, Ames W, Pantazis DA, Rapatskiy L, Lohmiller T, Kulik LV, Dorlet P, Rutherford AW, Neese F, Boussac A, Lubitz W, Messinger J, Biochim. Biophys. Acta - Bioenergetics 2011, 1807, 829–840.

[11]. Cox N, Rapatskiy L, Su J-H, Pantazis DA, Sugiura M, Kulik L, Dorlet P, Rutherford AW, Neese F, Boussac A, Lubitz W, Messinger J, J. Am. Chem. Soc 2011, 133, 3635–3648. [PubMed: 21341708]

[12]. Rapatskiy L, Cox N, Savitsky A, Ames WM, Sander J, Nowaczyk MM, Rögner M, Boussac A, Neese F, Messinger J, Lubitz W, J. Am. Chem. Soc 2012, 134, 16619–16634. [PubMed: 22937979]

[13]. Pantazis DA, Ames W, Cox N, Lubitz W, Neese F, Angew. Chem. Int. Ed 2012, 51, 9935–9940.

[14]. Bovi D, Narzi D, Guidoni L, Angew. Chem. Int. Ed 2013, 52, 11744–11749.

[15]. Cox N, Retegan M, Neese F, Pantazis DA, Boussac A, Lubitz W, Science 2014, 345, 804. [PubMed: 25124437]

[16]. Oyala PH, Stich TA, Stull JA, Yu F, Pecoraro VL, Britt RD, Biochemistry 2014, 53, 7914–7928. [PubMed: 25441091]

[17]. Oyala PH, Stich TA, Debus RJ, Britt RD, J. Am. Chem. Soc 2015, 137, 8829–8837. [PubMed: 26083545]

[18]. Chatterjee R, Han G, Kern J, Gul S, Fuller FD, Garachtchenko A, Young ID, Weng T-C, Nordlund D, Alonso-Mori R, Bergmann U, Sokaras D, Hatakeyama M, Yachandra VK, Yano J, Chem. Sci 2016, 7, 5236–5248. [PubMed: 28044099]

[19]. Lohmiller T, Krewald V, Sedoud A, Rutherford AW, Neese F, Lubitz W, Pantazis DA, Cox N, J. Am. Chem. Soc 2017, 139, 14412–14424. [PubMed: 28921983]

[20]. Siegbahn PEM, Acc. Chem. Res 2009, 42, 1871–1880. [PubMed: 19856959]

[21]. Cox N, Pantazis DA, Neese F, Lubitz W, Acc. Chem. Res 2013, 46, 1588–1596. [PubMed: 23506074]

[22]. Pérez Navarro M, Ames WM, Nilsson H, Lohmiller T, Pantazis DA, Rapatskiy L, Nowaczyk MM, Neese F, Boussac A, Messinger J, Lubitz W, Cox N, Proc. Nat. Acad. Sci 2013, 110, 15561. [PubMed: 24023065]

[23]. Gupta R, Taguchi T, Lassalle-Kaiser B, Bominaar EL, Yano J, Hendrich MP, Borovik AS, Proc. Nat. Acad. Sci 2015, 112, 5319–5324. [PubMed: 25852147]

[24]. Corry TA, O'Malley PJ, J. Am. Chem. Soc 2020, 142, 10240–10243. [PubMed: 32431144]

[25]. Krewald V, Retegan M, Neese F, Lubitz W, Pantazis DA, Cox N, Inorg. Chem 2016, 55, 488–501. [PubMed: 26700960]

[26]. Kulik LV, Epel B, Lubitz W, Messinger J, J. Am. Chem. Soc 2007, 129, 13421–13435. [PubMed: 17927172]

[27]. Yamauchi T, Mino H, Matsukawa T, Kawamori A, Ono T.-a., Biochemistry 1997, 36, 7520–7526. [PubMed: 9200702]

[28]. Campbell KA, Gregor W, Pham DP, Peloquin JM, Debus RJ, Britt RD, Biochemistry 1998, 37, 5039–5045. [PubMed: 9548734]

[29]. Campbell KA, Peloquin JM, Pham DP, Debus RJ, Britt RD, J. Am. Chem. Soc 1998, 120, 447–448.

[30]. Boussac A, Un S, Horner O, Rutherford AW, Biochemistry 1998, 37, 4001–4007. [PubMed: 9565450]

[31]. Boussac A, Rutherford AW, Biochim. Biophys. Acta 2000, 1457, 145–156. [PubMed: 10773159]

[32]. Haddy A, Lakshmi KV, Brudvig GW, Frank HA, Biophys. J 2004, 87, 2885–2896. [PubMed: 15454478]

[33]. Morton J, Chrysina M, Craig VSJ, Akita F, Nakajima Y, Lubitz W, Cox N, Shen J-R, Krausz E, Biochim. Biophys. Acta - Bioenergetics 2018, 1859, 88–98. [PubMed: 29066392]

[34]. Marchiori DA, Debus RJ, Britt RD, Biochemistry 2020, 59, 4864–4872. [PubMed: 33319991]

[35]. Matsukawa T, Mino H, Yoneda D, Kawamori A, Biochemistry 1999, 38, 4072–4077. [PubMed: 10194321]

[36]. Chatterjee R, Lassalle L, Gul S, Fuller FD, Young ID, Ibrahim M, de Lichtenberg C, Cheah MH, Zouni A, Messinger J, Yachandra VK, Kern J, Yano J, Physiologia Plantarum 2019, 166, 60–72. [PubMed: 30793319]

[37]. Kanady JS, Tsui EY, Day MW, Agapie T, Science 2011, 333, 733. [PubMed: 21817047]

[38]. Kanady JS, Mendoza-Cortes JL, Tsui EY, Nielsen RJ, Goddard WA, Agapie T, J. Am. Chem. Soc 2013, 135, 1073–1082. [PubMed: 23241061]

[39]. Isobe H, Shoji M, Yamanaka S, Mino H, Umena Y, Kawakami K, Kamiya N, Shen JR, Yamaguchi K, Phys. Chem. Chem. Phys 2014, 16, 11911–11923. [PubMed: 24632787]

[40]. Chrysina M, Heyno E, Kutin Y, Reus M, Nilsson H, Nowaczyk MM, DeBeer S, Neese F, Messinger J, Lubitz W, Cox N, Proc. Nat. Acad. Sci 2019, 116, 16841. [PubMed: 31391299]

[41]. Boussac A, Ugur I, Marion A, Sugiura M, Kaila VRI, Rutherford AW, Biochim. Biophys. Acta - Bioenergetics 2018, 1859, 342–356. [PubMed: 29499187]

[42]. Boussac A, Rutherford AW, Sugiura M, Biochim. Biophys. Acta - Bioenergetics 2015, 1847, 576–586.

[43]. Pokhrel R, Brudvig GW, Phys. Chem. Chem. Phys 2014, 16, 11812–11821. [PubMed: 24700294]

[44]. Lee HB, Marchiori DA, Chatterjee R, Oyala PH, Yano J, Britt RD, Agapie T, J. Am. Chem. Soc 2020, 142, 3753–3761. [PubMed: 32013412]

[45]. Mukhopadhyay S, Mandal SK, Bhaduri S, Armstrong WH, Chem. Rev 2004, 104, 3981–4026. [PubMed: 15352784]

[46]. Mishra A, Wernsdorfer W, Abboud KA, Christou G, Chem. Commun 2005, 54–56.

[47]. Hewitt IJ, Tang J-K, Madhu NT, Clérac R, Buth G, Anson CE, Powell AK, Chem. Commun 2006, 2650–2652.

[48]. Mullins CS, Pecoraro VL, Coord. Chem. Rev 2008, 252, 416–443. [PubMed: 19081816]

[49]. Mukherjee S, Stull JA, Yano J, Stamatatos TC, Pringouri K, Stich TA, Abboud KA, Britt RD, Yachandra VK, Christou G, Proc. Nat. Acad. Sci 2012, 109, 2257. [PubMed: 22308383]

[50]. Tsui EY, Agapie T, Proc. Nat. Acad. Sci 2013, 110, 10084. [PubMed: 23744039]

[51]. Tsui EY, Kanady JS, Agapie T, Inorg. Chem 2013, 52, 13833–13848. [PubMed: 24328344]

[52]. Tsui EY, Tran R, Yano J, Agapie T, Nat. Chem 2013, 5, 293. [PubMed: 23511417]

[53]. Zhang C, Chen C, Dong H, Shen J-R, Dau H, Zhao J, Science 2015, 348, 690–693. [PubMed: 25954008]

[54]. Lin P-H, Takase MK, Agapie T, Inorg. Chem 2015, 54, 59–64. [PubMed: 25521310]

[55]. Lee HB, Tsui EY, Agapie T, Chem. Commun 2017, 53, 6832–6835.

[56]. Paul S, Neese F, Pantazis DA, Green Chem. 2017, 19, 2309–2325.

[57]. Chen C, Chen Y, Yao R, Li Y, Zhang C, Angew. Chem. Int. Ed 2019, 58, 3939–3942.

[58]. Lee HB, Agapie T, Inorg. Chem 2019, 58, 14998–15003. [PubMed: 31095368]

[59]. Hagen KS, Westmoreland TD, Scott MJ, Armstrong WH, J. Am. Chem. Soc 1989, 111, 1907–1909.

[60]. Baldwin MJ, Stemmler TL, Riggs-Gelasco PJ, Kirk ML, Penner-Hahn JE, Pecoraro VL, J. Am. Chem. Soc 1994, 116, 11349–11356.

[61]. Krewald V, Lassalle-Kaiser B, Boron TT, Pollock CJ, Kern J, Beckwith MA, Yachandra VK, Pecoraro VL, Yano J, Neese F, DeBeer S, Inorg. Chem 2013, 52, 12904–12914. [PubMed: 24161030]

[62]. Lassalle-Kaiser B, Boron TT, Krewald V, Kern J, Beckwith MA, Delgado-Jaime MU, Schroeder H, Alonso-Mori R, Nordlund D, Weng T-C, Sokaras D, Neese F, Bergmann U, Yachandra VK, DeBeer S, Pecoraro VL, Yano J, Inorg. Chem 2013, 52, 12915–12922. [PubMed: 24161081]

[63]. Mathe Z, Pantazis DA, Lee HB, Gnewkow R, Van Kuiken BE, Agapie T, DeBeer S, Inorg. Chem 2019, 58, 16292–16301. [PubMed: 31743026]

[64]. Krewald V, Neese F, Pantazis DA, J. Am. Chem. Soc 2013, 135, 5726–5739. [PubMed: 23527603]

[65]. Lee HB, Shiau AA, Oyala PH, Marchiori DA, Gul S, Chatterjee R, Yano J, Britt RD, Agapie T, J. Am. Chem. Soc 2018, 140, 17175–17187. [PubMed: 30407806]

[66]. Lin P-H, Tsui EY, Habib F, Murugesu M, Agapie T, Inorg. Chem 2016, 55, 6095–6099. [PubMed: 27281290]

[67]. Kanady JS, Lin P-H, Carsch KM, Nielsen RJ, Takase MK, Goddard WA, Agapie T, J. Am. Chem. Soc 2014, 136, 14373–14376. [PubMed: 25241826]

[68]. Jones CG, Asay M, Kim LJ, Kleinsasser JF, Saha A, Fulton TJ, Berkley KR, Cascio D, Malyutin AG, Conley MP, Stoltz BM, Lavallo V, Rodríguez JA, Nelson HM, ACS Central Science 2019, 5, 1507–1513. [PubMed: 31572777]

[69]. Baffert C, Orio M, Pantazis DA, Duboc C, Blackman AG, Blondin G, Neese F, Deronzier A, Collomb M-N, Inorg. Chem 2009, 48, 10281–10288. [PubMed: 19795871]

[70]. Pei Y, Journaux Y, Kahn O, Inorg. Chem 1988, 27, 399–404.

[71]. Ribas J, Diaz C, Costa R, Journaux Y, Mathoniere C, Kahn O, Gleizes A, Inorg. Chem 1990, 29, 2042–2047.

[72]. Gao E-Q, Tang J-K, Liao D-Z, Jiang Z-H, Yan S-P, Wang G-L, Inorg. Chem 2001, 40, 3134–3140. [PubMed: 11399184]

[73]. Chaudhuri P, Coord. Chem. Rev 2003, 243, 143–190.

[74]. Jeon I-R, Park JG, Xiao DJ, Harris TD, J. Am. Chem. Soc 2013, 135, 16845–16848. [PubMed: 24164631]

[75]. DeGayner JA, Jeon I-R, Harris TD, Chem. Sci 2015, 6, 6639–6648. [PubMed: 29435213]

[76]. Sánchez RH, Betley TA, J. Am. Chem. Soc 2018, 140, 16792–16806. [PubMed: 30403845]

[77]. Boča R, Coord. Chem. Rev 2004, 248, 757–815.

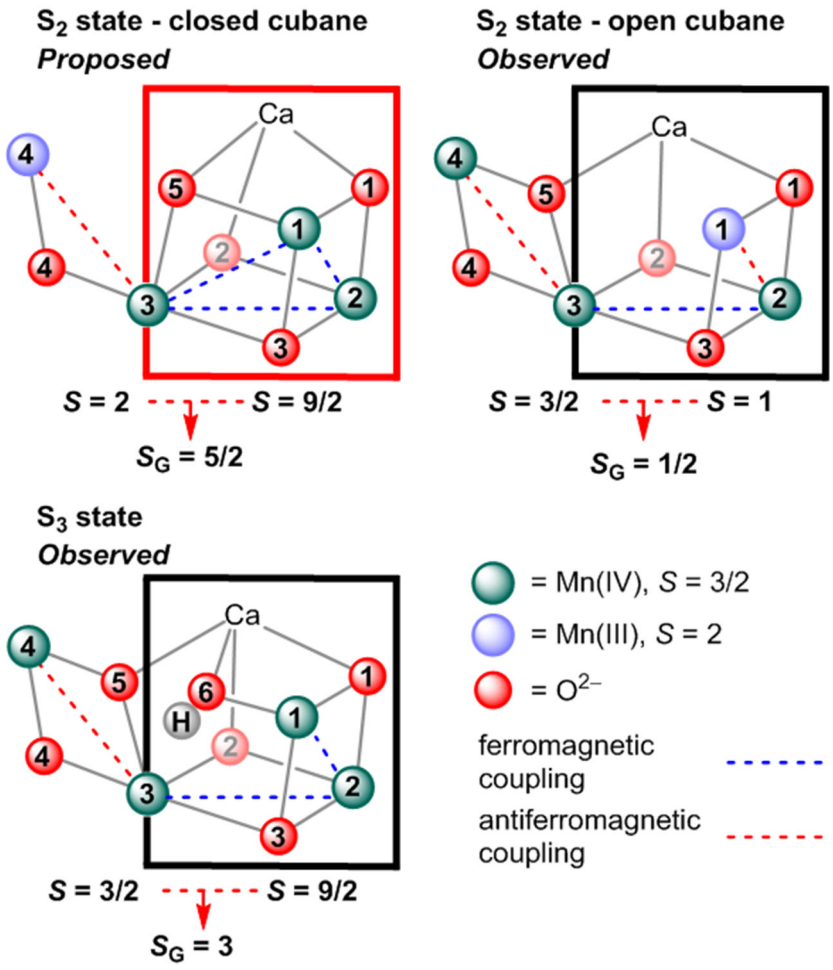

Figure 1.

Proposed or observed structures of the inorganic $CaMn_4$ core of the OEC in the S_2 and S_3 states. Trinuclear subsites boxed for emphasis, especially the proposed closed cubane motif in red, which is the focus of this study. Nature of the calculated magnetic exchange coupling interactions shown in red (antiferromagnetic) and blue (ferromagnetic) dashed lines. Coupling between Mn(4) and the trinuclear subsite leads to the observed spin ground states S_G.

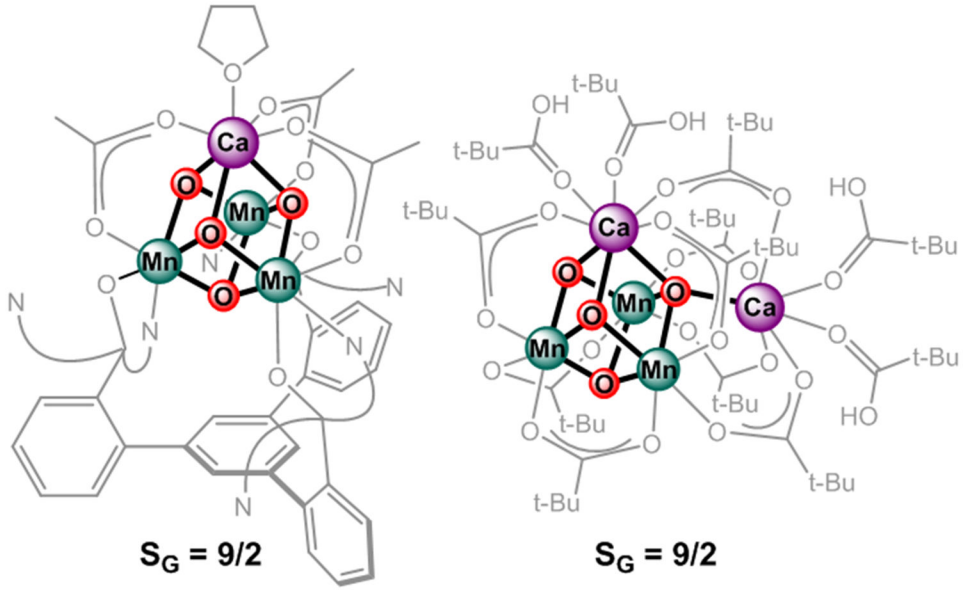

Figure 2.
Previously reported complexes featuring a $CaMn_3^{IV}O_4$ core.

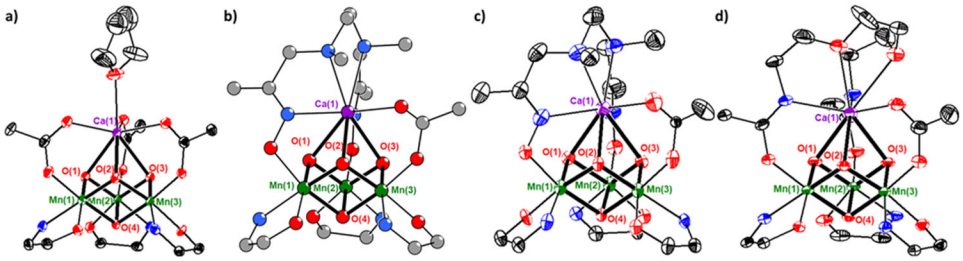

Figure 3.

Truncated crystal structures of a) **1-Ca**,[37] b) **2-Ca**, c) **3-Ca**,[67] d) **4-Ca**. Ellipsoids at 50% probability except for **2-Ca** (ball and stick model).

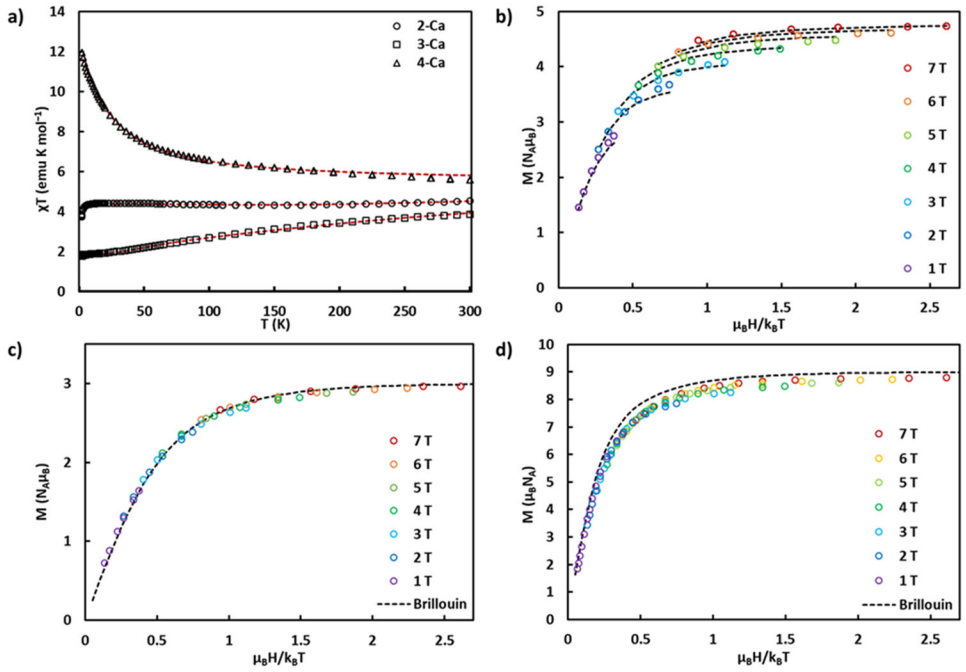

Figure 4.

a) XT vs. T plot of complexes **2-Ca**, **3-Ca**, and **4-Ca** with corresponding fits to the data. b)–d) Reduced magnetization plot of **2-Ca**, **3-Ca**, and **4-Ca**, respectively. See text for fit parameters.

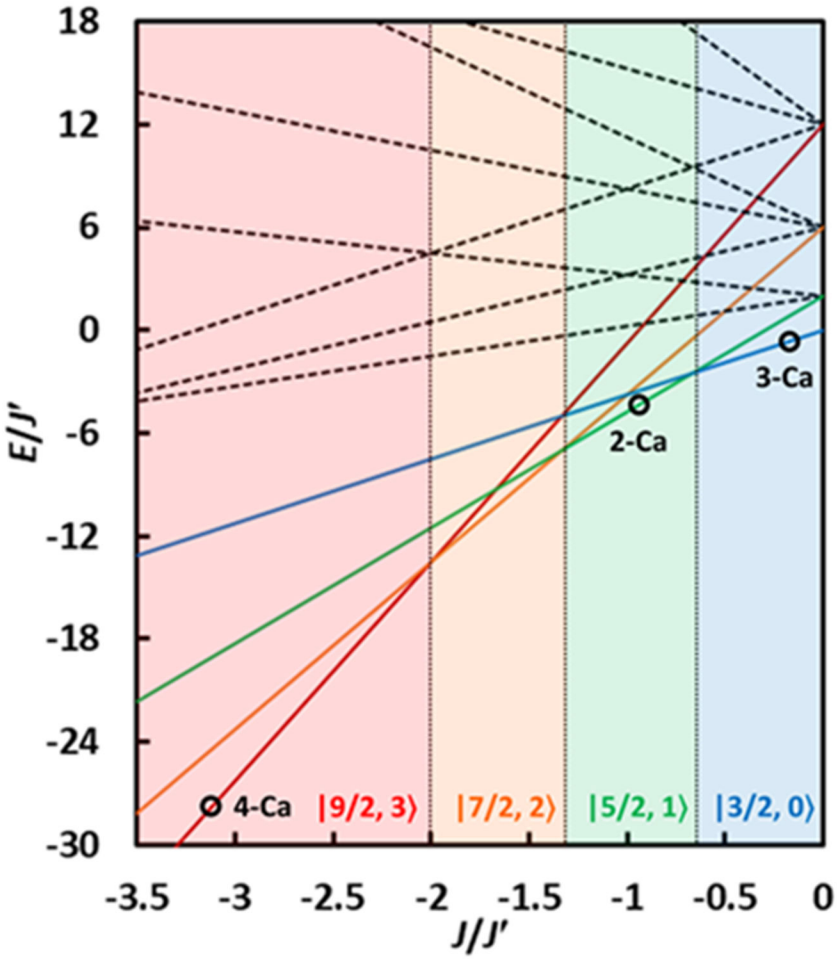

Figure 5.

Relative energies E/J' of the $|S_T, S\rangle$ states as a function of J/J' (for $J' < 0$). Each colored region represents a different spin ground state. Experimental points shown as black circles.

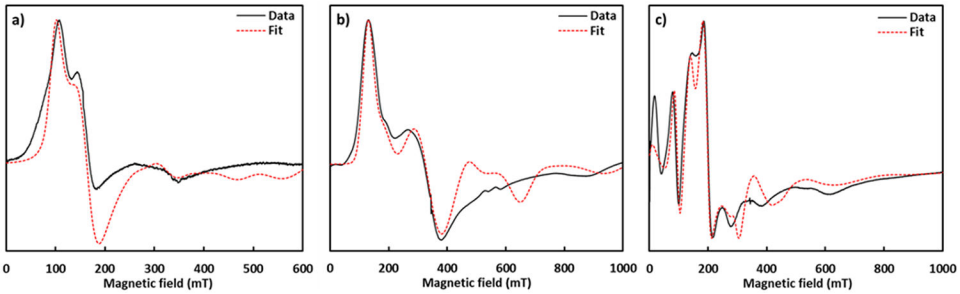

Figure 6.

X-band EPR spectra collected at 5 K (black traces) and corresponding simulations (dashed red traces). a) **2-Ca**, $S = 5/2$, $g = 1.96$, $D = 0.3\ cm^{-1}$, $E/D = 0.06$, fwhm E/D distribution 0.03. b) **3-Ca**, $S = 3/2$, $g = 1.98$, $D = 0.28\ cm^{-1}$, $E/D = 0.33$. c) **4-Ca**, $S = 9/2$, $g = 1.99$, $D = -0.1\ cm^{-1}$, $E/D = 0.11$.

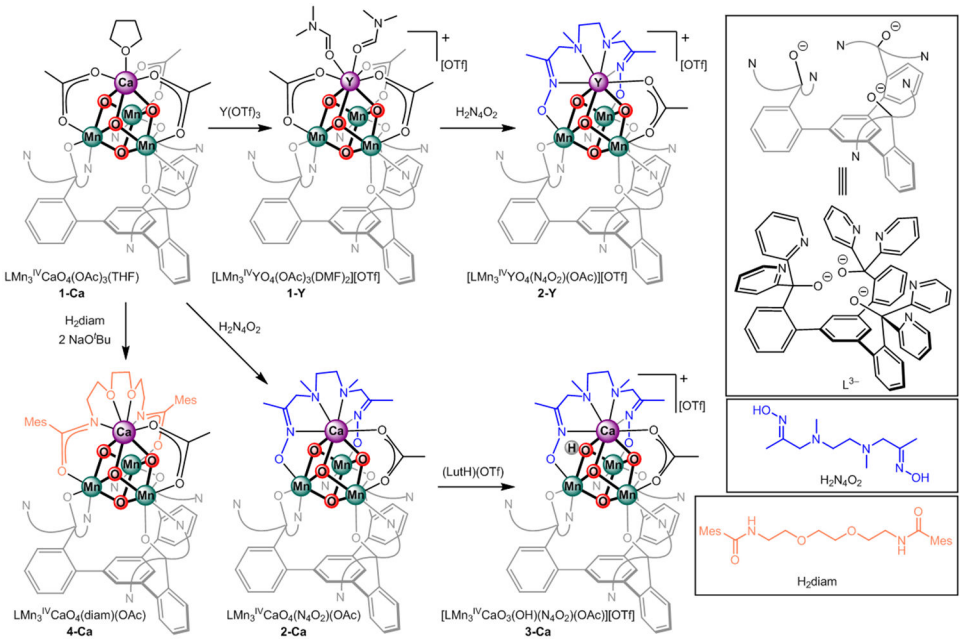

Scheme 1.
Synthesis of complexes studied in this work.